Supplementary Information

Impact of deoxygenation and hydrological changes on the Black Sea nitrogen cycle during the Last Deglaciation and Holocene

Anna Cutmore[1*]., Nicole Bale[1]., Rick Hennekam[2]., Darci Rush[1]., Bingjie Yang[1]., Gert-Jan Reichart[2,3]., Ellen C. Hopmans[2]., Stefan Schouten[1,3]

[1]Department of Marine Microbiology & Biogeochemistry, NIOZ Royal Netherlands Institute for Sea Research

[2]Department of Ocean Systems, NIOZ Royal Netherlands Institute for Sea Research

[3]Department of Earth Sciences, Universiteit Utrecht

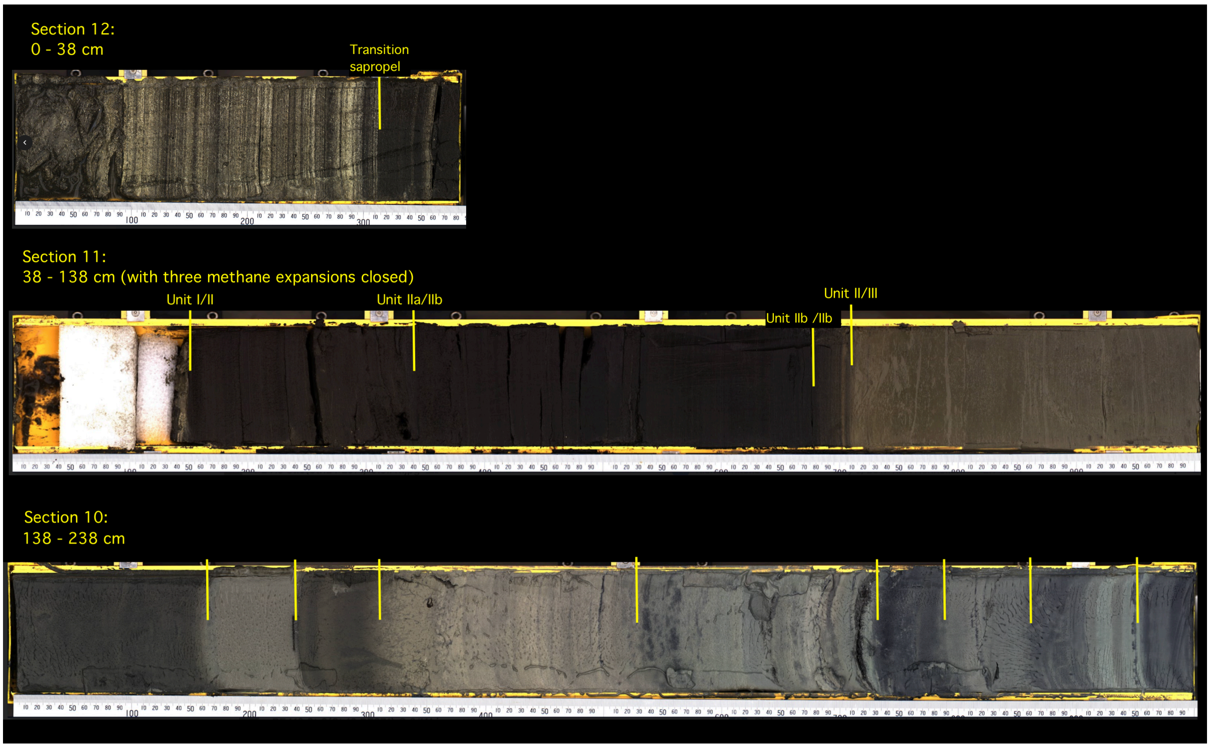

Figure S1: Scan of core 64PE418 showing colour changes and the depth of unit boundaries. Unit boundaries are defined according to Arthur & Dean (1998) and have been identified by colour changes and XRF-core-scan changes in Ti and Ca (Fig. S3).

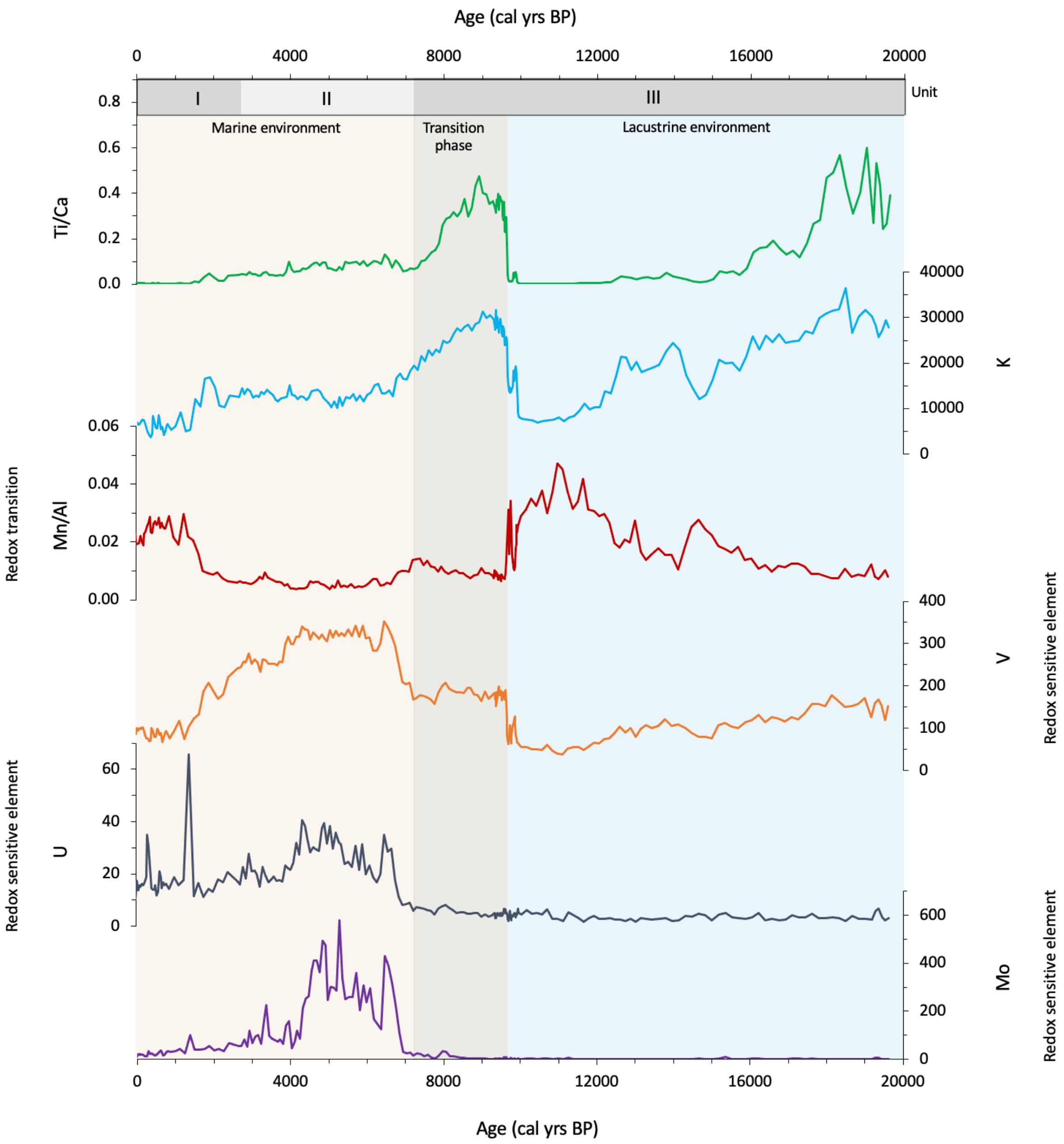

Figure S2: Changes over the last 19.6 ka in the elemental content of core 64PE418, as measured through calibrated XRF-core-scanning (ppm) using the methods described in Hennekam et al. (2020).

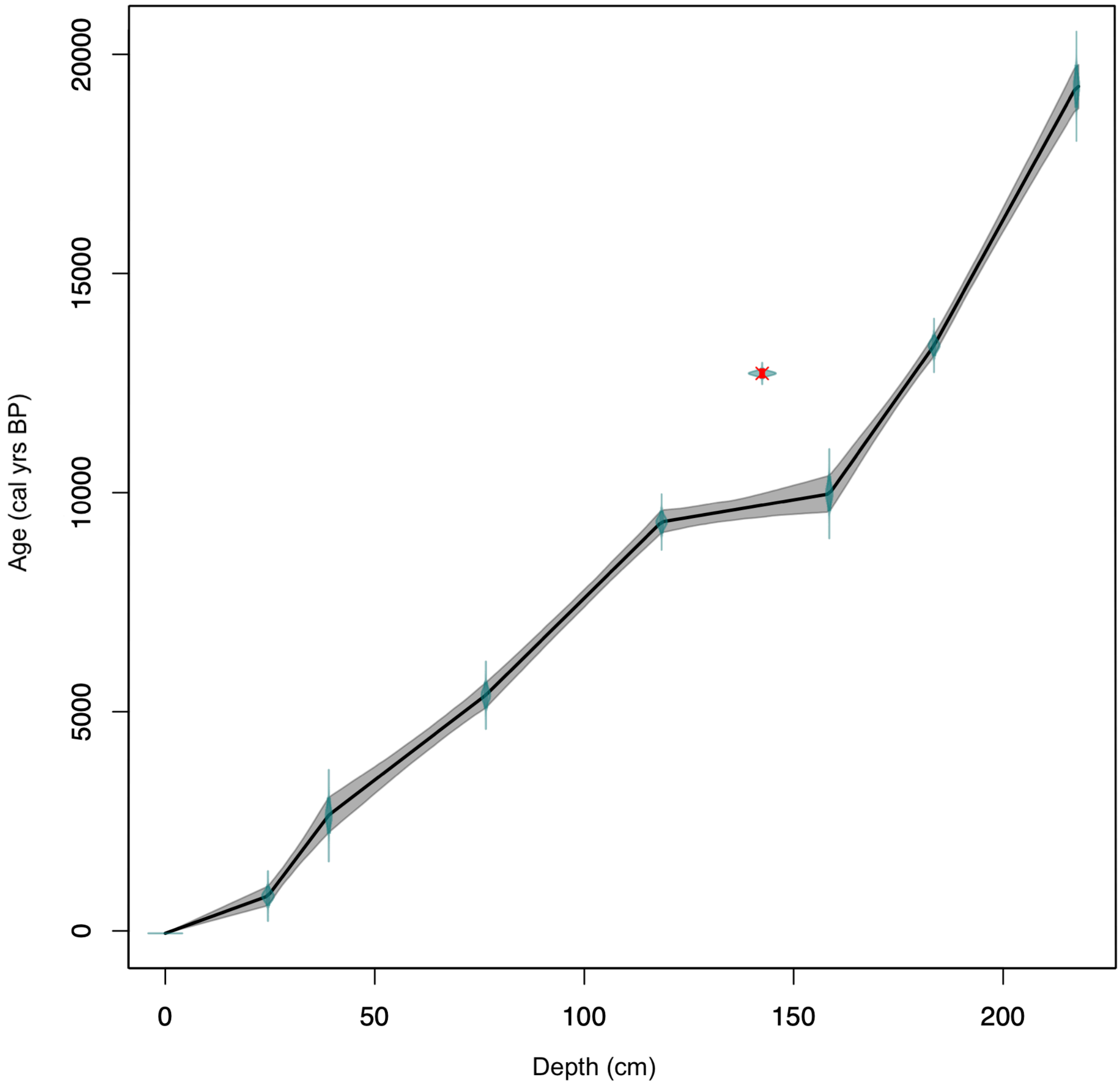

Figure S3: Age-depth model for core 64PE418, created using seven ^{14}C dates, six from core 64PE418 and one from KNR134-08-BC17 (Jones & Gagnon, 1994). Red dot shows the one excluded ^{14}C date at 142.5 cm due to an age-reversal.

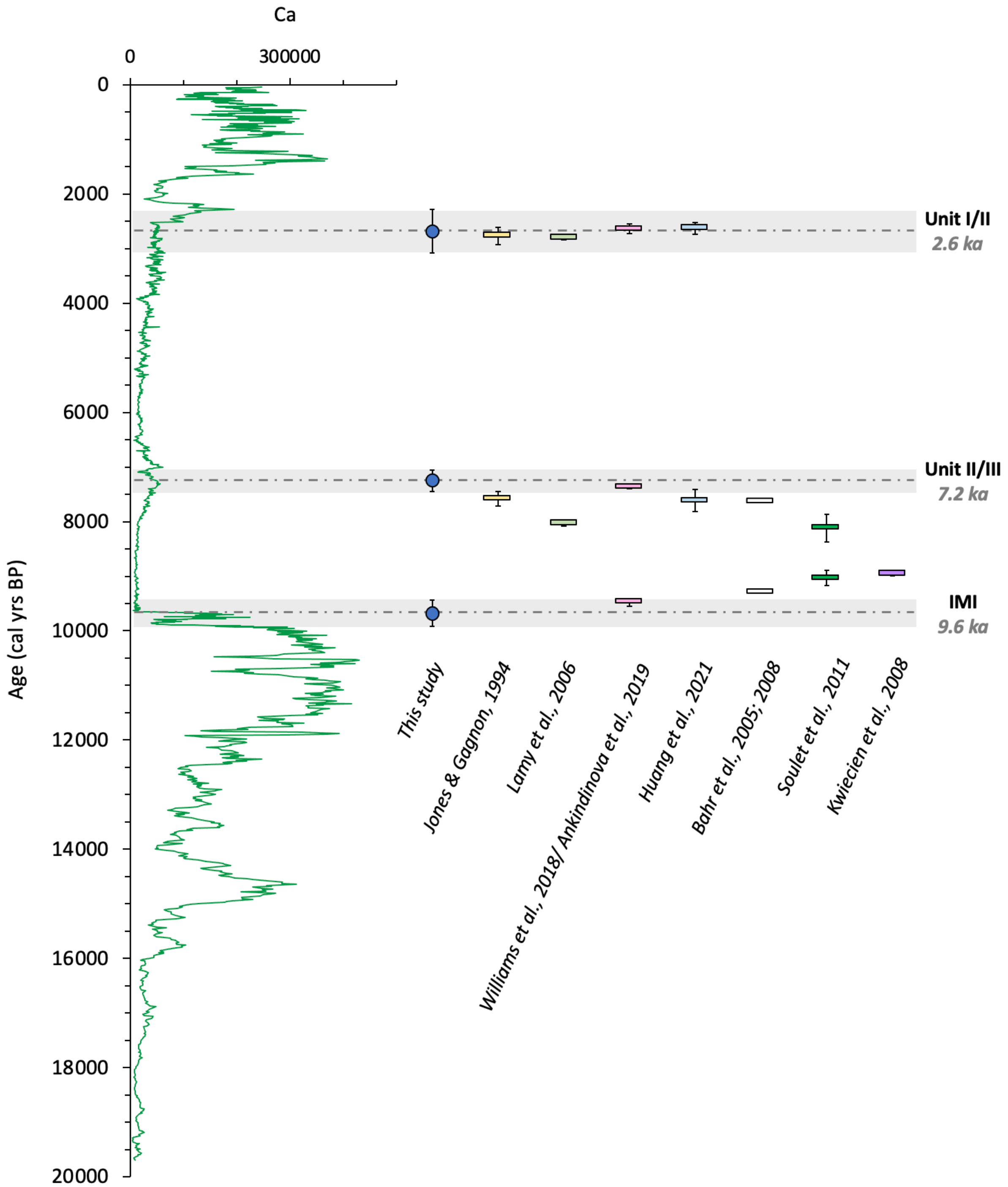

Figure S4: Calibrated ^{14}C ages of the key transitions in core 64PE418 over the Holocene (grey dashed lines, with error shown by grey band), and alignment with the previously published calibrated ages of these boundaries from existing studies (Jones & Gagnon, 1994; Lamy et al., 2006; Williams et al., 2018; Akindinova et al., 2019; Huang et al., 2021; Bahr et al., 2005; 2008; Soulet et al., 2011; Kwiecien et al., 2008), also highlighting their errors. Ca record from this study is also shown, in green.

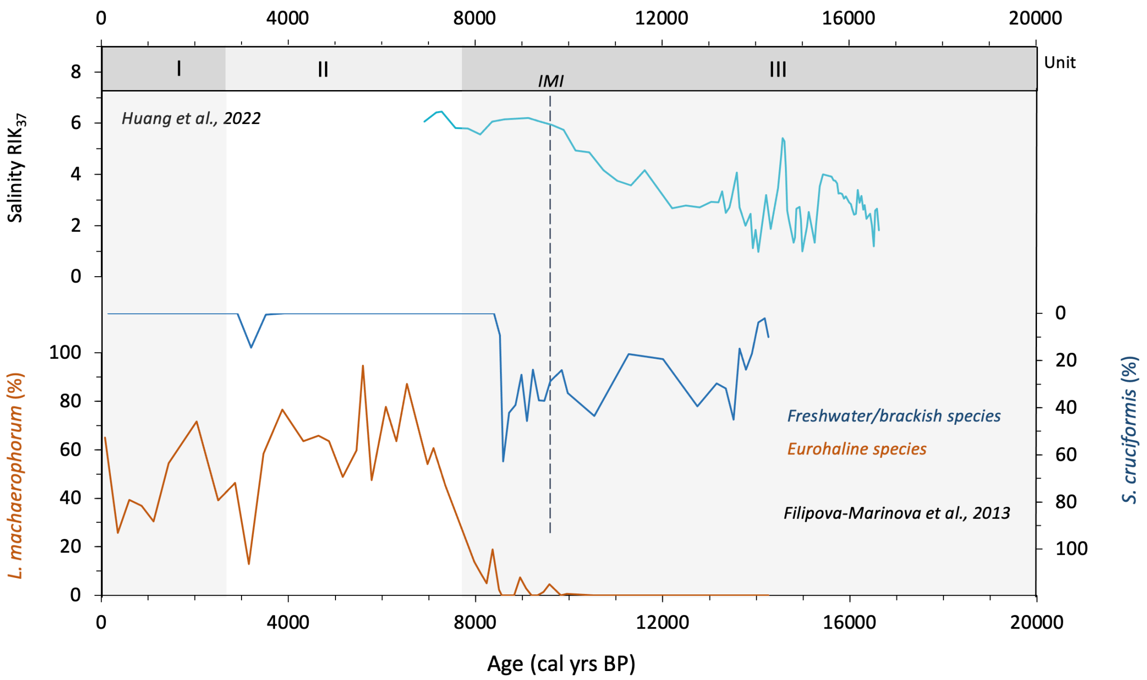

Figure S5: Salinity reconstructions of the Black Sea over the Last Deglaciation and Holocene using RIK$_{37}$ (Huang et al., 2022) and dinocysts (Filipova-Marinova et al., 2013).

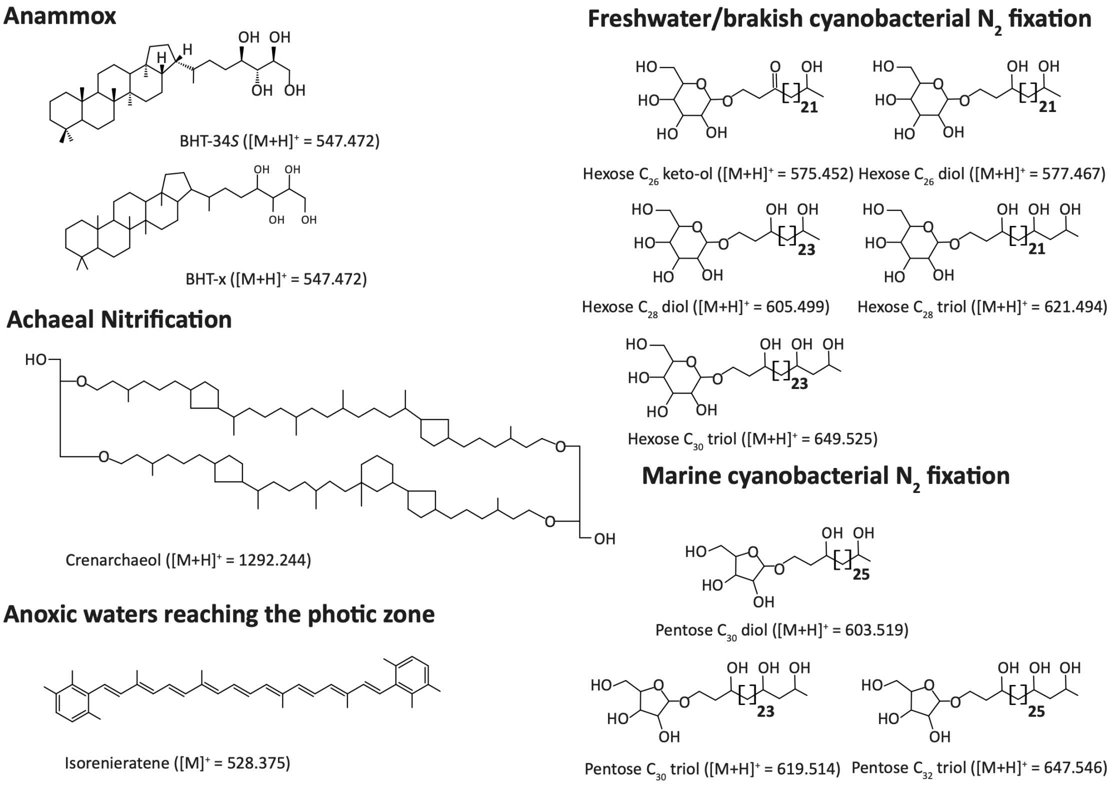

Figure S6: Chemical structures of the lipid biomarkers used in this study to explore past changes in the Black Sea N-cycle. Note that crenarchaeol is drawn in the anti-parallel structure but also occurs in the parallel structure.

	Retention time (min)	Accurate mass ($[M+H]^+$)		AEC	Δ mmu	CFI
		Calculated	Observed			
Crenarchaeol[a]	66.8	1292.2444	1292.2452	$C_{86}H_{163}O_6$	0.8	n/a
Isorenieratene[a]	28.6	528.3751[e]	528.3754[e]	$C_{40}H_{48}$	0.3	133.1012, 436.3123
BHT-34S[a]	20.41	529.4615[f]	529.4610	$C_{35}H_{61}O_3$	0.5	163.148, 191.179
BHT-x[a]	20.82	529.4615[f]	529.4636	$C_{35}H_{61}O_3$	2.1	163.148, 191.179
H C_{26} diol[a]	10.2	577.4674	577.4677	$C_{32}H_{65}O_8$	0.3	361.3826, 379.3930, 398.4033, 415.4141
H C_{28} diol[b]	12.0	605.4987	605.4995	$C_{34}H_{69}O_8$	0.8	389.4138, 407.4224, 425.4348, 443.4454
H C_{28} triol[c]	9.2	621.4936	621.4933	$C_{34}H_{69}O_9$	0.3	387.3973, 405.4085, 423.4189, 441.4308, 459.4402
H C_{30} triol[c]	11.1	649.5249	649.5247	$C_{36}H_{73}O_9$	0.2	451.451, 469.4615, 487.4721
P C_{30} diol[d]	14.1	603.5198	603.5194	$C_{35}H_{71}O_7$	0.4	417.4456, 435.4558, 453.4673, 471.4760
P C_{30} triol[d]	11.7	619.5143	619.5148	$C_{35}H_{71}O_8$	0.5	415.4293, 433.4400, 451.4504, 469.4611, 487.4718
P C_{32} triol[d]	13.3	647.5456	647.5458	$C_{37}H_{74}O_8$	0.2	443.4605, 461.4713, 479.4815, 497.4922, 515.5029

[a] Data from depth 135 cm
[b] Data from depth 130 cm
[c] Data from depth 160 cm
[d] Data from depth 13 cm
[e] $[M]^+$ ion in place of $[M+H]^+$
[f] $[M+H]^+$-H_2O ion in place of $[M+H]^+$

Table S1. Identifying characteristics of the compounds reported in this study. AEC = assigned elemental composition, Δ mmu = (measured mass – calculated mass) x 1000 as calculated for extract from 1000 m depth. CFI = characteristic fragment ion(s). 135 cm

References:

Ankindinova, O., Hiscott, R.N., Aksu, A.E and Grimes, V. 2019. High-resolution Sr-isotopic evolution of Black Sea water during the Holocene: Implications for reconnection with the global ocean. *Marine Geology*, **407**, 213-228.

Bahr, A., Lamy, F., Arz, H., Kuhlmann, H and Wefer, G. 2005. Late glacial to Holocene climate and sedimentation history in the NW Black Sea. *Marine Geology*, **214**, 309-322.

Bahr, A., Lamy, F., Arz, H., Major, C., Kwiecien, O and Wefer, G. 2008. Abrupt changes of temperature and water chemistry in the late Pleistocene and early Holocene Black Sea. *Geochemistry, Geophysics, Geosystems*, **9**, 1-16.

Jones, G.A and Gagnon, A.R. 1994. Radiocarbon chronology of Black Sea sediments. *Deep-Sea Research 1*, **41**, 531-557.

Hennekam, R., van der Bolt, B., van Nes, E.H., de Lange, G.-J., Scheffer, M and Reichart, G.-J. 2020. Early-warning signals for marine anoxic events. *Geophysical Research Letters*, **47**, 1-9.

Huang, Y., Zheng, Y., Heng, P., Giosan, L and Coolen, M.J.L. 2021. Black Sea paleosalinity evolution since the last deglaciation reconstructed from alkenone-inferred Isochrysidales diversity. *Earth and Planetary Science Letters*, **564**, 1-9.

Kwiecien, O., Arz, H.W., Lamy, F., Wulf, S., Bahr, A., Röhl, U and Haug, G.H. 2008. Estimated Reservoir Ages of the Black Sea Since the Last Glacial. *Radiocarbon*, 50, 99-118.

Soulet, G., Ménot, G., Lericolais, G and Bard, E. 2011. A revised calendar age for the last reconnection of the Black Sea to the global ocean. *Quaternary Science Reviews*, **30**, 1019-1026.

Lamy, F., Arz, H.W., Bond, G.C., Bahr, A and Pätzold, J. 2006. Multicentennial-scale hydrological changes in the Black Sea and northern Red Sea during the Holocene and the Arctic/North Atlantic Oscillation. *Paleoceanography & Paleoclimatology*, **21**, 1-11.

Williams, L.R., Hiscott, R.N., Aksu, A.E., Bradley, L.R., Horne, D.J and Stoica, M. 2018. Holocene paleoecology and paleoceanography of the southwestern Black Sea shelf revealed by ostracod assemblages. *Marine Micropaleontology*, **142**, 48-66.